Development of a Stop-Rotor Unmanned Arial Vehicle (UAV)

Alvaro Vargas-Clara
Arizona State University
avargasc@asu.edu

Sangram Redkar
Arizona State University
sredkar@asu.edu

Abstract

The objective of this work is to develop a stop-rotor UAV. This UAV is capable of vertical takeoff and landing (VTOL) like a helicopter and can convert from a helicopter mode to an airplane mode in mid flight. Thus, this UAV can hover as a helicopter and achieve high mission ranges like an airplane. The stop-rotor implies that in mid flight the lift generating helicopter rotor stops and the rotor blades transform into airplane wings. The thrust in the airplane mode is provided by a pusher propeller. This aircraft configuration presents unique challenges in modeling, aerodynamics, and control. Another important task is to design an autopilot for this configuration that will stabilize the aircraft and fly by wire. In this paper we present, modeling, aircraft design and briefly discuss the autopilot architecture of this UAV. We also present some experimental "conversion" results where the stop-rotor aircraft was dropped from a hot air balloon and performed successful conversions from helicopter to airplane mode and vice versa.

Introduction

The Wright Brothers achieved successful powered heavier than air flight because the critical issue they solved was control – not the recognition of the simplification offered by separating lift from propulsion which was already recognized since Sir George Cayley's (1773-1857) time. Of course, yaw and pitch control were already resolved by Cayley's cruciform rudder. However, the remaining critical issue of roll control was not practically solved by Otto Lilienthal and others using shifting weight. Successful powered heavier than air flight was not possible until the Wrights solved roll control with wing warping. Fixed wing aircraft performance has since far eclipsed those humble beginnings at Kitty Hawk. Similarly, rotary wing developments have also far eclipsed the modest flight performances pioneered by Sikorsky, Piasecki and others.

For any meaningful payload, speed, and endurance, airplanes need runways. Helicopters, featuring no need for runways, cannot compare with their fixed wing relatives for payload, speed, range, or endurance. A vehicle that would not require a runway like a helicopter but enjoy the payload, speed, range, and endurance of an airplane would be an ideal aircraft. The

multi mode rotors on tilt-rotor vehicles, such as the V-22 Osprey and the TR911D Eagle Eye UAV, are compromised in terms of blade twist, geometry, et cetera, due to conflicting requirements depending on the mode of flight. In cruise as a fixed wing, the rotors are far from ideal as a thrust device; and while in helicopter mode, the rotors are likewise far from ideal in hover and particularly in autorotation. Such fundamental compromises will likely make a candidate tilt-rotor small VTOL UAV performance fall well short of the mission range and endurance performance objectives over fixed wing (citing the Scan Eagle example) and gain the VTOL capability. For over five decades, the aerospace community has recognized that such an ideal aircraft would likely be a stop rotor configuration. For most of those five decades, innumerable stop rotor concepts and ideas have been advanced. Among recent efforts have been the cancelled Boeing X-50 Canard Rotor Wing and the Sikorsky X-Wing.

In virtually every case known to the authors, the stop rotor concepts were of a radial flow conversion category. This is to say the rotor disc is parallel to the airflow during conversion when the rotors are to be slowed and stopped to become wings. Like the roll control critical issue plaguing airplane developers fifty years since Cayley's experiments, the stop rotor development progress has been stalled for fifty years mainly over the obstacle of the conversion approach between rotary and fixed wing modes of flight. What is demonstrably needed to resolve this critical issue hampering stop rotor development is a departure from the radial flow conversion approach. Stop-rotor, a stop rotor proposed herein, is the first and only stop rotor concept where an axial flow conversion approach is advanced. Axial flow conversion is analogous to feathering or pitching propellers with the airflow impinging upon the rotor disc plane perpendicularly, aligned with the rotational axis of the rotor. The principal advantage of an axial flow conversion approach compared to the radial flow conversion is the airflow impinging the airfoil does not change direction – so the airfoil can have conventional, normal profiles with aero-elastically stable quarter chord pitch axes.

A radial flow conversion stop rotor, in sharp contrast, forces the airfoil to experience ~180º changes in direction of the airflow on the airfoil during conversion between rotary and fixed wing flight modes. This is because on the retreating blade side, the rotor's trailing edge becomes a leading edge when locked in the fixed wing position. This has resulted in very serious compromises and consequences including 50% chord-wise pitching axis placement; creating considerable aero-elasticity problems including flutter, and a one per revolution oscillatory center of lift during conversion. All of these and other problems and similar challenges encountered have proven to be virtually insurmountable by radial flow conversion stop rotor design approaches.

The Flight Conversion Concept for the stop-rotor is illustrated in figure 1. It is important to note that the stop-rotor can convert between helicopter and airplane modes of flight any number of times during the same flight. The helicopter mode is not just the launch and recovery method that some have misunderstood from this illustration. Really, the point of this illustration is to emphasize the conversion sequence between helicopter and airplane mode of flight for the vehicle.

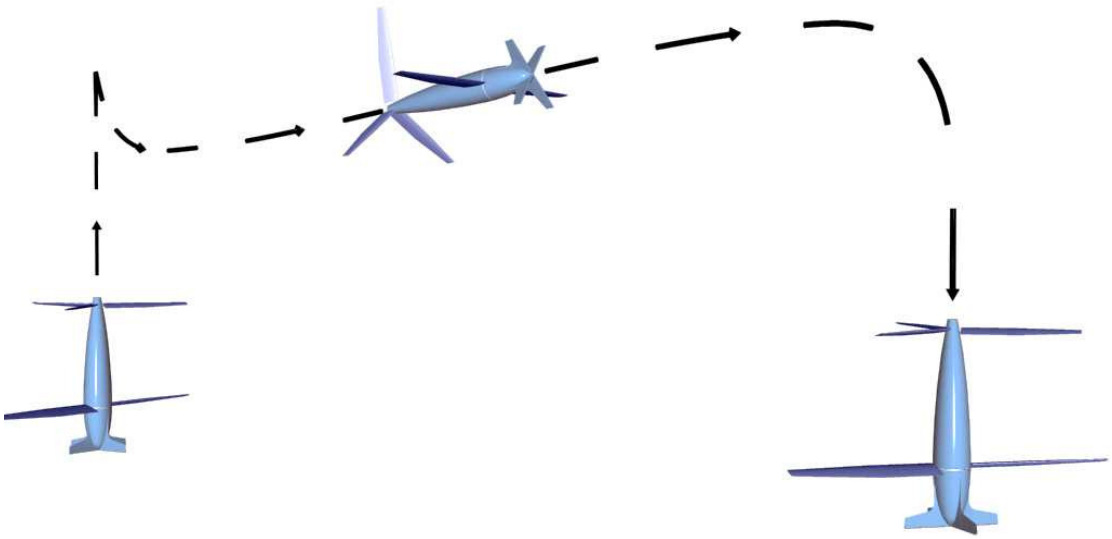

Figure 1: Stop-rotor Flight Conversion

For example, from the powered helicopter mode a selectable clutch is released while the wings and tail fins are collectively pitched (analogous to feathering a propeller) until in the airplane mode position. The wings and tail fins stop rotation solely due to external aerodynamic forces and do not require indexing or braking and/or locking mechanism of any kind. The selectable clutch engages the propeller drive shaft and power is now delivered to the pusher propeller for airplane mode of flight. The propeller is thus optimized for cruise and not compromised like so many fixed pitch propeller UAVs for take-off and cruise conditions. In Airplane to Helicopter (from powered airplane) mode the clutch is released and the wing and tailfins are collectively pitched to the autorotation position. The wings and tail fins spin up solely due to external aerodynamic forces. The selectable clutch engages the tail fin hub and power is then delivered to the tail fin for powered helicopter mode of flight while the collective pitch is increased to provide hovering and normal helicopter-like flight in the usual manner. Thus, the stop-rotor is an ideal fixed wing, uncompromised in terms of propulsion and landing mechanism making available higher weight fractions for payload and fuel for longer endurance and greater payload than conventional fixed wing. In helicopter mode, stop-rotor is an ideal rotary wing vehicle, with efficient, slow turning rotors without a power-robbing tail rotor for anti-torque.

In this paper we present, mathematical modeling of the UAV, design considerations, experimental results, and a brief discussion on the autopilot. The discussion and conclusion are included at the end.

Mathematical modeling of the Stop-rotor

Consider the stop-rotor as shown in figure 2. In order to develop the mathematical model, stop-rotor structure is divided into following subcomponents.

a) Tail rotor: Tail rotor comprises of three identical tail fins. It acts as a rotor in the helicopter mode and generates lift.
b) Wings: The wings provide the lift in the airplane mode and have control surfaces. In the helicopter mode, the wings rotate due to torque reaction.
c) Fuselage: Fuselage houses the electro-optical payload and is stationary during helicopter or aircraft mode.

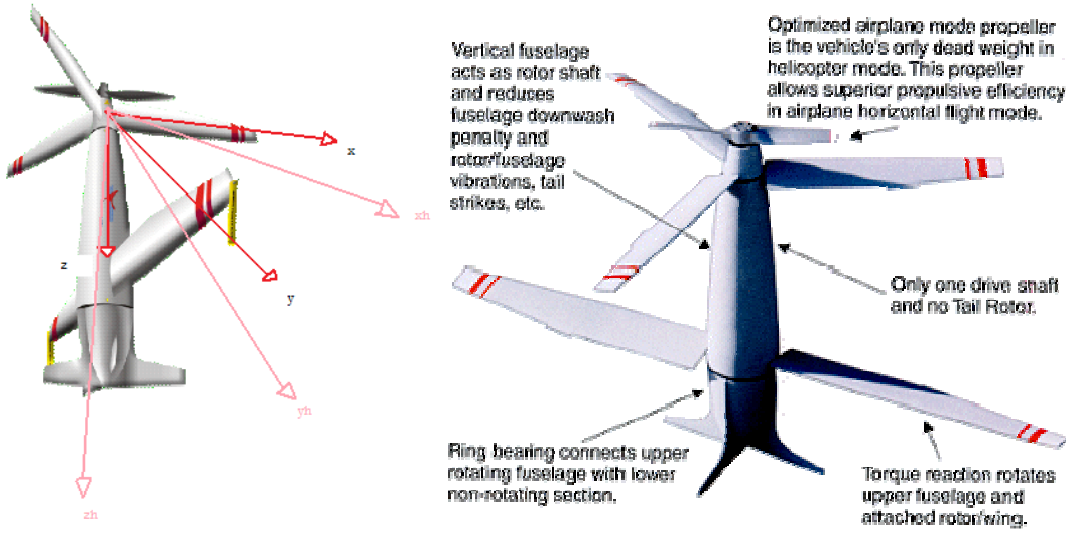

Figure 2: Stop-rotor configuration & coordinate axes

In this section, the mathematical model of the stop-rotor is briefly discussed. This model is incorporated in the MATLAB code. The mathematical model for the is developed using d'Alembert's principle considering dynamic, gravity, and aerodynamic forces [1-3]. For the initial analysis, Stop-rotor tail rotor is assumed unpowered and conversion from helicopter mode to airplane mode is achieved by feathering the wings. Following coordinate systems are used to develop the model as shown in Figure 2.

1. Tail rotor body-fixed coordinate system that rotates with tail rotor.
2. Hub co-ordinate system coinciding with the tail-rotor coordinate system but fixed to hub.
3. Wing co-ordinate system: wing fixed coordinate system rotating with wing in the helicopter mode.
4. Gravity co-ordinate system: located on fuselage coinciding with the hub coordinate system but z axis is always pointed towards gravity.
5. Ground coordinate system -inertial coordinate system located fixed on ground.

We follow prodecure similar to the procedure presented in references 1-3 to derive the equations of motion. The gravity coordinate system is translated from the ground coordinate system with $\mathbf{x} = [x_G, y_G, z_G]$; where x_G, y_G, z_G correspond to distances from the inertial reference frame. The relation between the coordinates in both the systems is given by

$$\mathbf{x}_p = \mathbf{A}(\psi, \theta, \phi)\mathbf{x} \qquad (1)$$

where $\mathbf{A}(\psi, \theta, \phi)$ is the generalized rotation matrix and ψ, θ, ϕ are inertial yaw, pitch and roll angles.

Equations of motion for the Stop-rotor are grouped as

$$\begin{aligned} \mathbf{F}_{TR} + \mathbf{F}_F + \mathbf{F}_W &= 0 \\ \mathbf{M}_{TR} + \mathbf{M}_W + \mathbf{M}_W &= 0 \end{aligned} \tag{2}$$

where $\mathbf{F}_{TR}, \mathbf{F}_F, \mathbf{F}_W$ are the forces acting on tail rotor, fuselage and wings, $\mathbf{M}_{TR}, \mathbf{M}_W, \mathbf{M}_W$ are the moments acting on tail rotor, fuselage and wings. Each element of equation (2) comprises of inertia, aerodynamic and gravity parts.

Inertial Loads: The expressions for inertial load $\mathbf{Q}_{pi}$ is obtained using the conservation of momentum, which can be written in the general form as

$$\mathbf{Q}_{pi} = \mathbf{I}_{pi}(\dot{\mathbf{Y}}_{pi} + \dot{\mathbf{Y}}_{mi}) + (\boldsymbol{\Omega}_{pi} + \boldsymbol{\Omega}_{mi})\mathbf{I}_{pi}(\mathbf{Y}_{pi} + \mathbf{Y}_{mi}) \tag{3}$$

where $\mathbf{I}_{pi}$ is the generalized inertia matrix, $\mathbf{Y}_{pi}$ is the state vector comprising or components of velocities and rates. $\mathbf{Y}_{mi}$ is the state vector comprising of the relative velocities and rates. $\boldsymbol{\Omega}_{pi}, \boldsymbol{\Omega}_{mi}$ are angular velocities and relative angular velocity matrices. The nonlinear parts of equation (3) contains all acceleration acting on the rotating elements including gyroscopic effects.

Gravity Loads: The vector of gravity acceleration in the gravity coordinate system is given by $\mathbf{g} = [0, 0, g]^T$. The gravity vector can be rotated using the transformation matrix $\mathbf{A}_G(\psi, \theta, \phi)$. The gravity loads on Stop-rotor components can be calculated as

$$\begin{aligned} \mathbf{F}_{ig} &= m_i \mathbf{A}_G \mathbf{g} \\ \mathbf{M}_{ig} &= \mathbf{r}_{CG} \times (m_i \mathbf{A}_G \mathbf{g}) \end{aligned} \tag{4}$$

where m_i is the mass of the element/component and $\mathbf{r}_{CG}$ is the position vector from center of gravity of the element relative to reference coordinate frame.

Aerodynamic Loads: The differential aerodynamic loads comprising of Drag, Lift and Moment on element i can be expressed in the element coordinate system as

$$\begin{aligned} dD &= \frac{1}{2}\rho c(y) V_a^2 C_D(\alpha) dy \\ dL &= \frac{1}{2}\rho c(y) V_a^2 C_L(\alpha) dy \\ dM &= \frac{1}{2}\rho c^2(y) V_a^2 C_M(\alpha) dy \end{aligned} \tag{5}$$

where $\frac{1}{2}\rho V_a^2$ is the dynamic pressure and $C_D(\alpha), C_L(\alpha), C_M(\alpha)$ are coefficients of drag, lift and moment, respectively. The aerodynamic forces in the element coordinate system can be transformed to the coordinate system corresponding to equation (2). It is important to note that the tail fin and wing has NACA0012 airfoil, which is widely studied and performance data is available in literature. However, to characterize fuselage aerodynamic coefficients, CFD modeling, and/or wind tunnel testing is required.

Design Considerations

In the course of detailed design, Finite Element (FE) Analysis was used. In this section aerodynamic and FE analysis on the stop-rotor wing is briefly presented for details we refer to reference 4. A wing under operating conditions experiences aerodynamic loads. These aerodynamic loads were used to conduct a structural analysis on the wing structure of the Spin Wing. The wing was pin supported at two bearing locations at aluminum spar. The loads that the wing structure experienced were lift force, drag force, and moment. All aerodynamic loads were assumed to be acting at quarter chord point and to be constant along span of the wing.

The first step in conducting this analysis was to determine the aerodynamic loads that the wing structure would experience. These loads were determined by conducting a 2D CFD analysis on a NACA 0012 airfoil. The calculated Reynolds number the wing would operate was 483,908 at STP. The CFD analysis was conducted using XFLR 5 [5] software. In doing the CFD analysis, coefficients of lift, drag, and moment were obtained at various angles of attack. Once obtaining these coefficients, the aerodynamic forces were calculated using equation (5).

Table 1: Coefficient of Lift, Drag and Moment at different angles of attack [4]

Alpha	**CL**	**CD**	**CM**
0	0	0.00623	0
5	0.6317	0.01049	-0.0134
10	1.0411	0.01955	0.0114
15	1.2194	0.04987	0.0331

Table 2: Aerodynamic loads at different angles of attack [4]

Alpha	**Lift per unit Span(N/m)**	**Drag per unit Span (N/m)**	**Moment per unit Span(Nm)**
0	0	0.7196791	0
5	72.97292	1.2117871	-0.41284
10	120.2661	2.2583831	0.35122
15	140.863	5.7608984	1.019769

The next step was to construct the wing structure using Solidworks [6]. The structure is shown in figure 3, consisted of two major components, an airfoil skin and the aluminum spar. The span of the wing was 47.5 inches and the thickness was assumed to be 0.1 inches. The aluminum spar had a span of 52.5 inches and the thickness of the aluminum spar was measured to be 0.125 inches. The material for both components was assumed to be Aluminum 2014.

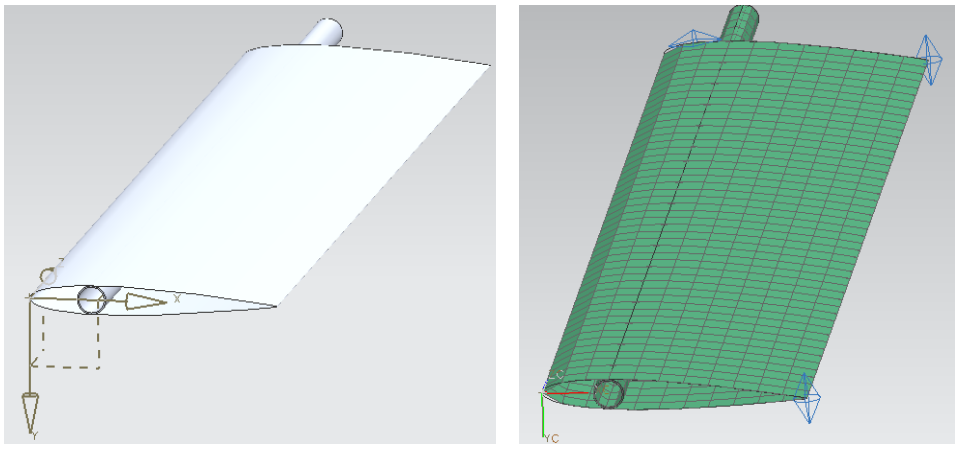

Figure 3: Wing structure and FE mesh [2]

The wing structure was then inputted into NX 7 Nastran [7] where mesh, constraints, and loads were applied. The elements selected for this analysis were thin shell Quad-4, and solid Hex-8. The airfoil skin used the thin shell while the aluminum spar used solid elements. A 2D mapped mesh was applied on the airfoil skin while a 3D swept mesh was applied on the aluminum cross section. This resulted in a uniform mesh in the aluminum spar and airfoil as shown in figure 3. A face split was used on the top surface of the airfoil to create a single contact point with the aluminum spar. At this location, the spar and airfoil shared common nodes along the span wise direction.

The last step to setting up the analysis was to input the loads and constraints. The edge created by the face split was used to apply the lift and drag forces. The lift force was applied on the top surface of the airfoil skin in the negative y-direction, while the drag force was split in half and applied in the top and bottom of the spar in the x-direction. The moment was applied in the inner surface of the tube in the z-direction. The constraints used for this analysis were pinned constraints at the aluminum spar. These constraints were selected to simulate the mounting structure of the wing. The method of applying these constraints was using a user defined constraint. This was done by fixing the translations in the x, y, and z direction in selected nodes at the locations where the bearing supports would be located.

Results

For this structural analysis the results obtained were for deflection, Von Mises stresses, and vibration of the wing structure. This analysis was conducted using the maximum values of lift, drag, and moment forces previously obtained. The wing structure had a maximum magnitude deflection of 0.167 inches located at the tip of the wing (as shown in figure 4). The minimum deflection was 0 inches situated at the constraints.

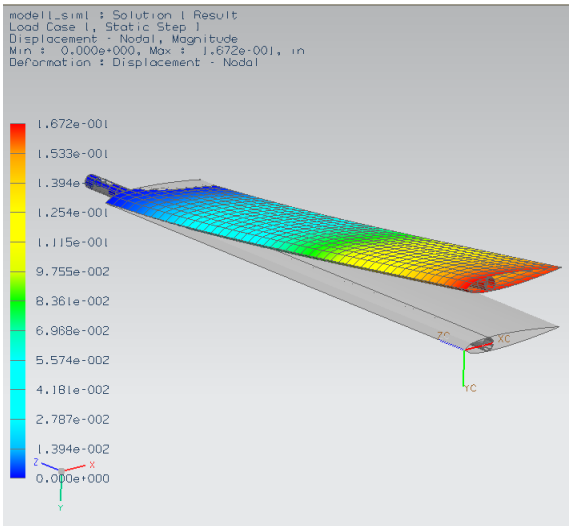

Figure 4: Magnitude Deflection of wing structure [4]

The maximum and minimum deflection in the x and y directions are given in the table 3:

Table 3: Max and min deflection in x and y direction [4]

Direction	**Maximum**	**Minimum**
X-direction	0.002243 in.	-0.00029 in.
Y-direction	0.1672 in.	-0.00675 in.

The maximum Von-Mises stress was obtained to be 5,421 psi located next to the pinned constraint, while the minimum Von-Mises stress was 1.931 psi at the tip of wing. These results are presented in figure 5.

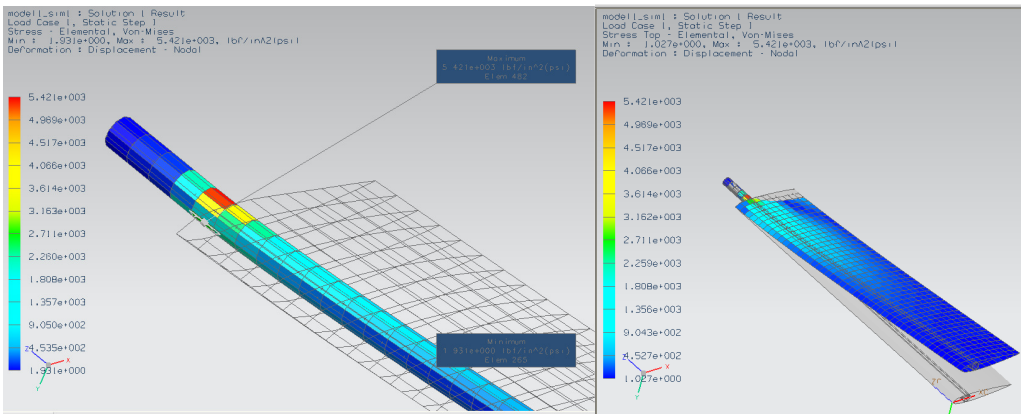

Figure 5 : Von Mises Stress in entire wing structure [4]

The maximum Von-Mises stress occurred at the bottom and top of the spar right after the constraints, this is understandable since the wing structure is mostly experiencing a bending due to the lift. As well, the maximum stress 5,421 psi is well within the yield strength of Aluminum 2014 which is 60,000 psi. This relative low Von-Mises value is due to the weak loading conditions the structure experienced. The aerodynamic forces were calculated using the assumption the max velocity the wing would experience is 26.82 m/s, which is a qualified small velocity. So the aerodynamic forces were small. The results obtained from vibration are realistic because it illustrated all of the deformations that are expected under vibration. The stop-rotor wing exhibits the following modes as shown in Table 4. These modes are depicted in Figure 6.

Table 4: Vibration deformations [4]

Vibration Frequency	**Deformation Type**
Mode 1: 15.9 Hz	Bending
Mode 2: 19.6 Hz	Lead or Drag
Mode 3: 71 Hz	Torsion
Mode 4: 112.5 Hz	Second Bending
Mode 5: 168.3 Hz	Second Torsion

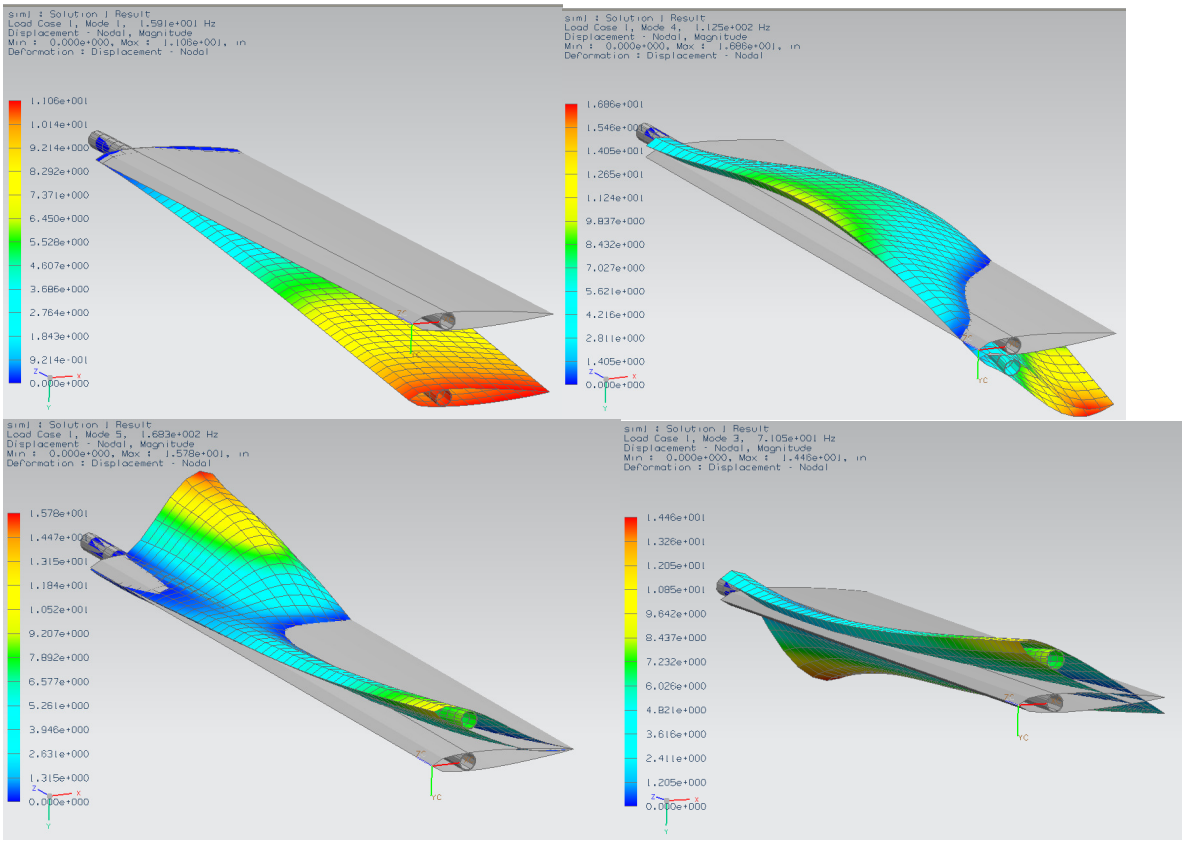

Figure 6: Stop-rotor Wing Vibration Modes [2]

Air frame Fabrication and Autopilot

After design validation, a test stand and airframe was fabricated in collaboration with local industry as shown in figure 7.

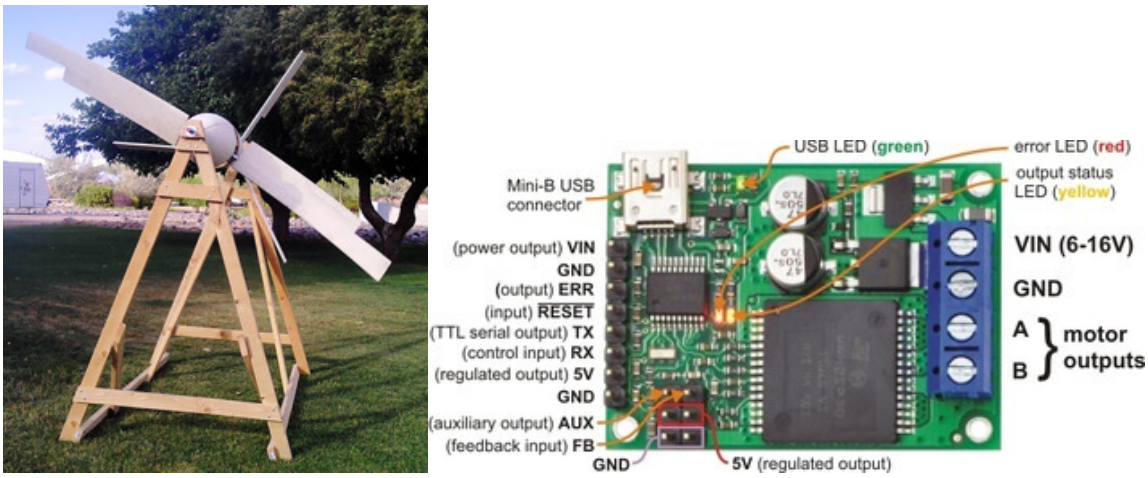

Figure 7: Stop-rotor Test Stand and Motor controller [9] for wing control

Collective feathering of the wing is the most important aspect of this design that enables the aircraft to transition from rotary wing to fixed wing configuration and vice versa. The wing collective control is obtained by two independent motor controllers shown in figure 7. Each controller is powered by separate battery pack. An RC interface is provided for collective and aileron control. Following fail-safe mechanism were incorporated in the wing collective control.

a. Electronic overrun stop
b. Mechanical overrun stop
c. Current limiting control

These electro-mechanical controls would ensure that the Stop-rotor will not lose control and wings would return to trim conditions in case of an overrun.

In order to log the data from the test instrumentation based on an open source autopilot Ardupilot was used [8]. This instrumentation comprises of an autopilot that has static and pitot pressure sensor, thermopiles and GPS. This autopilot used in data logging mode along with zigbee wireless transmitter and receiver, and a ground station as shown in figure 8. It is anticipated that this instrumentation will be used as an autopilot for Stop-rotor UAV later.

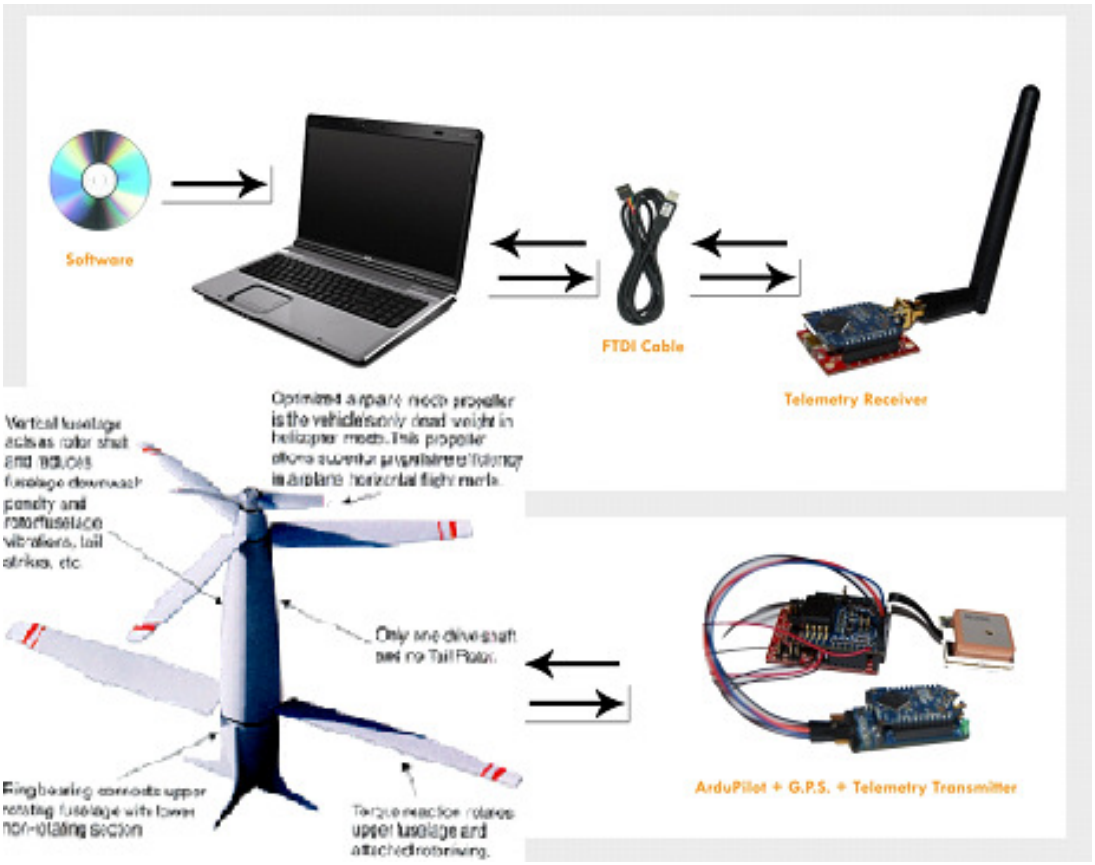

Figure 8: Ardupilot [8] Interface for Stop-rotor

The ground station interface was implemented using open source software [8] however; the Labview interface was modified to incorporate data logging capability as shown in figure 9. This ground station interface shows airspeed, GPS location, attitude, and altitude of the aircraft.

Figure 9: Ground Station Interface for Stop-rotor [8]

Experimental Validation of Stop Rotor Conversion

In order to demonstrate the conversion a "big drop" test was scheduled. In this drop test an unpowered Stop-rotor test specimen from a hot air balloon with the wings and tail fins pitched for helicopter mode (for autorotation), then dump the collective (feather) to an airplane mode position for the wings and tail fins, pull out of the dive and glide before pushing over and pitching the wings and tail fins back into their previous helicopter mode positions and land as shown in figure 10. The ardupilot [8] was used for data logging and a simple mathematical model for computation of rotor speed in helicopter autorotation mode was used [1].

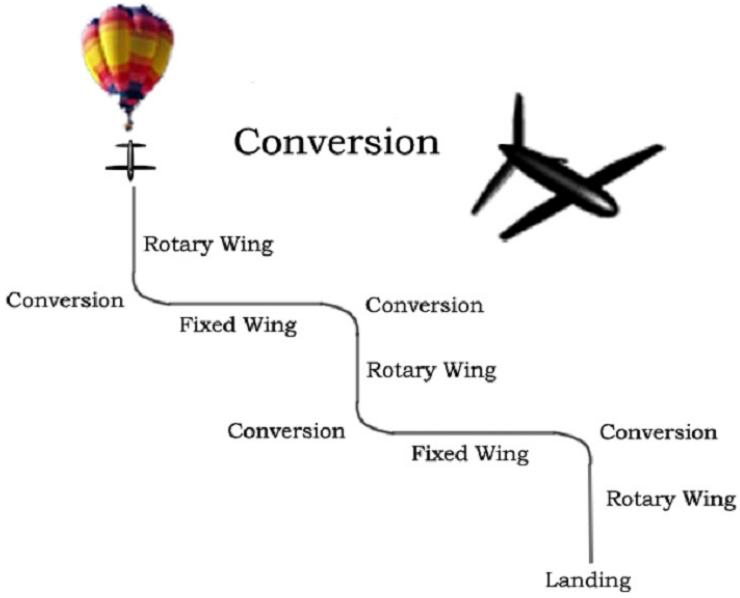

Figure 10: Stop-rotor Big Drop Test

It is noted that the big-drop is unpowered the expression for rotor speed in autorotation can be directly used to compute rotor RPM and velocity. These expression and their derivations are given in reference [1]. Thus, following the development from reference [1], we assume the first order equation for rotor speed

$$\mathbf{J}\dot{\Omega} = \mathbf{Q}_{eng} - \mathbf{Q}_{rotor} \tag{6}$$

Where $\mathbf{J}$ is the inertia, $\dot{\Omega}$ is the angular velocity, $\mathbf{Q}_{eng}, \mathbf{Q}_{rotor}$ are the engine torque and the rotor torque, respectively. The rotor torque $\mathbf{Q}_{rotor}$ and thrust $\mathbf{T}$ can be modeled as

$$\mathbf{Q}_{rotor} = \left(\frac{\Omega}{\Omega_0}\right)^2 \mathbf{Q}_0 \tag{7}$$

$$\mathbf{T} = \left(\frac{\Omega}{\Omega_0}\right)^2 \mathbf{W} \tag{8}$$

Where Ω_0 is the initial speed and $\mathbf{W}$ is the weight.

During the unpowered big drop, engine torque, $\mathbf{Q}_{eng} = 0$ and the rotor speed equation is given by

$$\mathbf{J}\dot{\Omega} = -\left(\frac{\Omega}{\Omega_0}\right)^2 \mathbf{Q}_0 \tag{9}$$

This is called Bernoulli's equation with the closed form solution

$$\Omega(t) = \frac{\Omega_0}{1 + \frac{\mathbf{Q}_0 t}{\mathbf{J}\Omega_0}} \tag{10}$$

The equation of vertical motion during the big drop (i.e. free fall) is given by

$$\ddot{y} = g(1 - \frac{\mathbf{T}}{\mathbf{W}}) = g[1 - \left(\frac{\Omega}{\Omega_0}\right)^2] \tag{11}$$

Equation (10) is substituted in equation (11) and integrated numerically once for velocity $\dot{y}$ and twice for position y determination. The simulation results by numerically integrating dynamical equations of motion and the experimental results are shown in figure 11. It is noted that initially from time t=2 sec. results, when the stop-rotor is in autorotation mode results are comparable. However, the difference between Expt. RPM and simulation RPM increases as the time increases. The difference between simulation and experimental results can be attributed to approximate aerodynamic modeling, approximate mathematical model for the stop-rotor, inability to specify exact initial condition during conversion and numerical integration error.

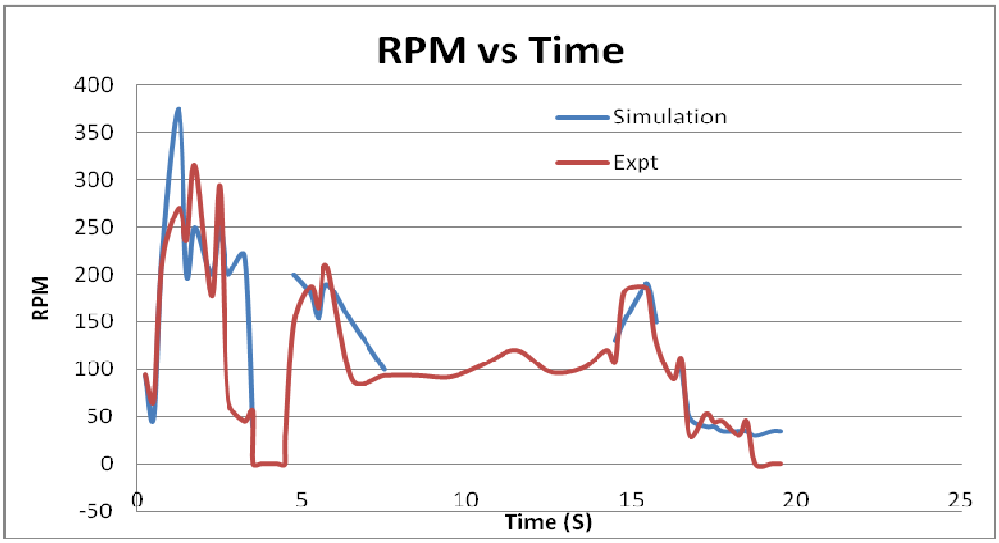

Figure 11: Comparison of simulation and experimental results

It can also be noted that during the drop from time t= 7 to14 seconds the stop-rotor has undergone an uncontrolled rolling (as shown in figure 32) in the fixed wing mode that results into the discontinuity in simulation RPM from time t=7 to14 seconds in figure 12.

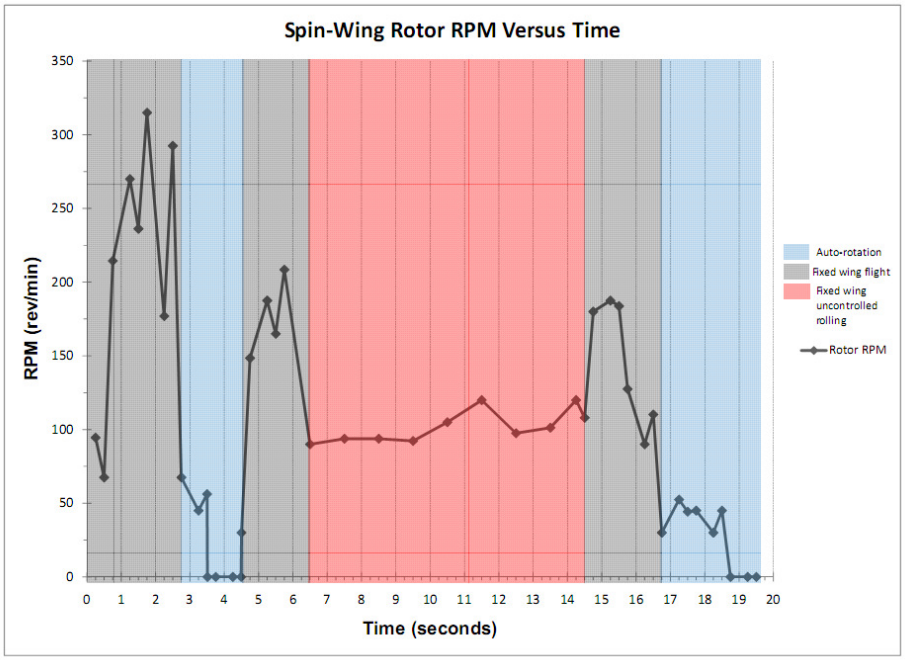

Figure 12: Stop-rotor Flight Modes during drop

Conclusion

In this work, modeling, analysis and drop test results on a novel stop rotor UAV is presented. A low cost, open source autopilot was used in a data-logging mode to acquire flight data. The results from a simple mathematical model of the drop test was compared with the experimental data. A successful helicopter to fixed wing flight conversion was demonstrated during the drop test. Currently, researchers at ASU are working on modifying modeling and simulation to yield more accurate fidelity with measurements.

Acknowledgment

The financial support from the Navy is gratefully acknowledged.

References

[1] M. Drier, Introduction to Helicopter and Tiltrotor Flight Simulation Published by AIAA, 2007, 1st Edition, ISBN-10: 1-56347-873-0, ISBN-13: 978-1-56347-873-4

[2] Kendoul, F. Fantoni, I. Lozano, R. "Modeling and Control of a Small Autonomous Aircraft Having Two Tilting Rotors"Robotics, IEEE Transactions on Volume: 22 Issue: 6, Dec. 2006 pp 1297 - 1302

[3] Ghiringhelli G.L; Masarati P.; Mantegazza P; Nixon M.W. " Multi-Body Analysis of a Tiltrotor Configuration",Nonlinear Dynamics, Volume 19, Number 4, August 1999 , pp. 333-357(25)

[4] A. Vargas-Clara, "Finite Element Analysis of Stop-rotor" Class Project Report, Spring 10.

[5] http://xflr5.sourceforge.net/xflr5.htm Retrived on 3/15/2011

[6] www.solidworks.com Retrived on 3/15/2011

[7] www.Siemens.com/NX Retrived on 3/15/2011

[8] http://www.pololu.com/catalog/product/1393 Retrived on 3/15/2011

[9] http://diydrones.com/notes/ArduPilot Retrived on 3/15/2011

Biography

ALVARO VARGAS-CLARA is a graduate student in the Department of Engineering Technology at ASU Poly.

SANGRAM REDKAR is an assistant professor in the Department of Engineering Technology at ASU Poly. His research interests include inertial measurement, MEMS dynamics, control, and nonlinear dynamics.